Excited state non-adiabatic dynamics of the smallest polyene, *trans* 1,3-butadiene. II. *Ab initio* multiple spawning simulations

William J. Glover,[1,2,3,4,5] Toshifumi Mori,[1,2,6,7] Michael S. Schuurman,[8,9] Andrey E. Boguslavskiy,[8,9,10] Oliver Schalk,[8,11] Albert Stolow,[8,9,10] and Todd J. Martínez[1,2,a)]

[1]*Department of Chemistry and The PULSE Institute, Stanford University, Stanford, California 94305, USA*
[2]*SLAC National Accelerator Laboratory, 2575 Sand Hill Road, Menlo Park, California 94025, USA*
[3]*NYU Shanghai, 1555 Century Avenue, Shanghai 200122, China*
[4]*NYU-ECNU Center for Computational Chemistry at NYU Shanghai, 3663 Zhongshan Road North, Shanghai 200062, China*
[5]*Department of Chemistry, New York University, New York, New York 10003, USA*
[6]*Institute for Molecular Science, Myodaji, Okazaki, Aichi 444-8585, Japan*
[7]*School of Physical Sciences, The Graduate University for Advanced Studies, Okazaki, Aichi 444-8585, Japan*
[8]*National Research Council Canada, 100 Sussex Drive, Ottawa, Ontario K1A 0R6, Canada*
[9]*Department of Chemistry, University of Ottawa, Ottawa, Ontario K1A 0R6, Canada*
[10]*Department of Physics, University of Ottawa, Ottawa, Ontario K1N 6N5, Canada*
[11]*Department of Physics, AlbaNova University Center, Stockholm University, 106 91 Stockholm, Sweden*

The excited state non-adiabatic dynamics of the smallest polyene, *trans* 1,3-butadiene (BD), has long been the subject of controversy due to its strong coupling, ultrafast time scales and the difficulties that theory faces in describing the relevant electronic states in a balanced fashion. Here we apply *Ab Initio* Multiple Spawning (AIMS) using state-averaged complete active space multistate second order perturbation theory [SA-3-CAS(4/4)-MSPT2] which describes both static and dynamic electron correlation effects, providing a balanced description of both the initially prepared bright 1^1B_u ($\pi\pi^*$) state and non-adiabatically coupled dark 2^1A_g state of BD. Importantly, AIMS allows for on-the-fly calculations of experimental observables. We validate our approach by directly simulating the time resolved photoelectron-photoion coincidence spectroscopy results presented in Paper I [A. E. Boguslavskiy *et al.*, J. Chem. Phys. **148**, 164302 (2018)], demonstrating excellent agreement with experiment. Our simulations reveal that the initial excitation to the 1^1B_u state rapidly evolves via wavepacket dynamics that follow both bright- and dark-state pathways as well as mixtures of these. In order to test the sensitivity of the AIMS results to the relative ordering of states, we considered two hypothetical scenarios biased toward either the bright ^1B_u or the dark 2^1A_g state. In contrast with AIMS/SA-3-CAS(4/4)-MSPT2 simulations, neither of these scenarios yields favorable agreement with experiment. Thus, we conclude that the excited state non-adiabatic dynamics in BD involves both of these ultrafast pathways.

I. INTRODUCTION

Cis-trans photoisomerization is an important photochemical transformation that converts light directly into mechanical motion on a nanometer length scale.[1–4] Nature has harnessed this energy conversion in a number of ways, a notable example being the photoisomerization of retinal as the primary step in vision.[5–7] Due to their apparently straightforward molecular structure, associated with a conjugated π backbone, the linear polyenes have become the paradigm for the study of photoisomerization. However, their apparent structural simplicity belies their complex excited state dynamics. Over the years, many mechanisms have been proposed to rationalize their observed photochemical products.[1–3,5,8–11] The excited state dynamics of the smallest unsaturated hydrocarbon, ethylene, is now relatively well understood.[12,13] However, the smallest polyene, *trans*-1,3-butadiene (BD), displays a remarkable complexity in its excited state dynamics and continues to be the subject of considerable controversy. In the preceding (Paper I[14]) and present (Paper II) papers, we detail our combined experimental-theoretical studies of BD excited to the optically bright $^1B_u(\pi\pi^*)$ state (S_2). In this paper, we describe our *ab initio* theoretical/computational study of excited state dynamics in BD using multireference perturbation theory [multistate second order perturbation theory (MSPT2)] for the electronic structure. This level of theory can describe both static and dynamic electron correlation effects, allowing for a balanced and accurate treatment of the various electronic states involved. Importantly, the *ab initio* calculation of time-resolved observables allows for direct comparison with the experimental time-resolved photoelectron spectroscopy (TRPES) and time-resolved photoelectron-photoion coincidence (TRPEPICO) spectroscopy results presented in the preceding paper,

a)Author to whom correspondence should be addressed: Todd.Martinez@stanford.edu

hereafter termed Paper I.[14] This combination of experiment with theory yields a complete description of the complex, ultrafast excited state dynamics of *trans*-1,3-butadiene.

As discussed previously by Levine and Martínez and references therein,[23] the disagreement over the mechanisms of excited state dynamics in BD stems in part from a historical controversy over the energetic ordering of its low-lying electronic states in the Franck-Condon (FC) region.[15] These are illustrated in Fig. 2 of Paper I.[14] The dominant determinants for the ground S_0 (1^1A_g) state and the first two excited states S_1/S_2 ($2^1A_g/1^1B_u$) of BD in C_{2h} symmetry are shown in Fig. 1. The 2^1A_g state is optically dark, and therefore its vertical excitation energy is hard to extract from experiment alone, adding to the controversy of the energetic ordering of states in this system. Furthermore, due to the multiconfigurational doubly excited character of the 2^1A_g state, most electronic structure methods find it difficult to produce a balanced description of the 2^1A_g and the 1^1B_u states. Previous models assuming that the initially populated bright 1^1B_u state was much lower in energy than the 2^1A_g state predicted that BD would decay via a localized one-bond-flip (OBF), much like ethylene.[8,16] By contrast, models assuming a reversed ordering of the 1^1B_u and 2^1A_g states predicted that BD would decay via a delocalized hula-twist (HT) mechanism,[1,3] similar to the longer polyenes.[10,17] Levine and Martínez explored the photodynamics of BD using a three-state-averaged complete active space self-consistent field with an active space of 4 electrons in 3 orbitals, SA-3-CASSCF(4/3), specifically chosen to give a balanced description of the 1^1B_u and 2^1A_g states. This gave rise to vertical excitation energies at the S_0 minimum of 7.87 eV and 7.92 eV.[23] Although these are ~1.5 eV higher than the experimental absorption maximum, the relative ordering and close energetic separation of these states agree with recent calculations at the equation-of-motion coupled-cluster singles doubles triples and quadruples level (EOM-CCSDTQ) that provided best estimates of 6.21 ± 0.02 eV and 6.39 ± 0.07 eV for the 1^1B_u and 2^1A_g states, respectively.[18] Performing *Ab Initio* Multiple Spawning (AIMS) calculations with SA-3-CASSCF(4/3), Levine and Martínez found that both one-bond-flip and hula-twist mechanisms were operative in the excited state dynamics of BD,[19] presumably due to the close energetic proximity of the 1^1B_u and 2^1A_g states. However, a quantitative prediction of the branching ratio between these paths was precluded since the calculations did not include dynamic electron correlation. This neglect of dynamic correlation is largely responsible for the ~1.5 eV blue shift of the excited electronic states compared to experiment. In order to ensure a correct description of the excited state non-adiabatic dynamics, one should include both static and dynamic electron correlation effects (which is what we do in this paper).

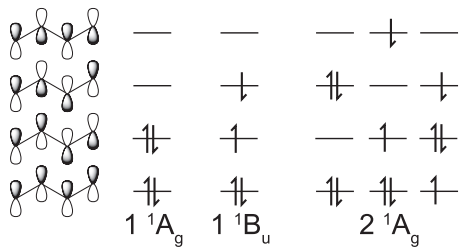

FIG. 1. Electronic structure of BD under C_{2h} symmetry, showing qualitatively the π molecular orbitals and predominant electron configurations for the lowest three electronic states.

Both dynamic and static electron correlation effects can be included with complete active space multistate second-order perturbation theory (MSPT2), and as we show in Table I (second column), MSPT2 yields BD vertical excitation energies which are in much better agreement with the EOM-CCSDTQ estimates.[18] Levine and Martínez showed that the shape of the PES using MSPT2 closely parallels that using CASSCF(4/3),[19] so one might expect a similar nonradiative decay mechanism. Evidence that this is the case can be found in the recent work of Komainda and co-workers who constructed a reduced six-[20] or eight-[21] dimensional vibronic Hamiltonian based on CASPT2 calculations and carried out wavepacket dynamics starting on the 1^1B_u state. They found that, similar to the work of Levine and Martínez,[19] out-of-plane torsion motions are important in bringing about the ultrafast 1^1B_u–2^1A_g non-adiabatic transition and in describing BD's very broad optical absorption spectrum.[20,21] Komainda and co-workers did not explore the S_1-S_0 non-adiabatic transition.

We recently interfaced the MSPT2 electronic structure with AIMS dynamics,[12,22–24] allowing for a full-dimensional multistate description of BD's non-radiative decay. The primary goal of the present study therefore is to revisit the excited state dynamics of BD using AIMS with the electronic structure determined using MSPT2 (calculated simultaneously with the dynamics, i.e., "on-the-fly"). This allows us to test the prediction that both bright state "ethylene-like" and dark state

TABLE I. Critical points of BD at three different levels of theory. The "reference" level is considered quantitatively accurate, while the "bright-biased" and "dark-biased" are employed to provide insight into the relative role of dark and bright states in the observed dynamics. Energies are given in eV relative to the ground-state equilibrium geometry. Ellipses indicate critical points that could not be located. Unless otherwise indicated, all geometries are optimized at the respective level of theory.

	SA-3-(4/4)-MSPT2 reference	SA-2-(2/2)-MSPT2 bright-biased	SA-2-(4/4)-MSPT2 dark-biased
1^1B_u vertical[a]	6.35	6.42	...
2^1A_g vertical[a]	6.47	...	6.46
2^1A_g planar minimum[b]	5.51	...	5.50
S_1 transoid minimum	...	...	4.68
C_s C^*[c]	5.49	...	5.63
C_s Me^-[c]	5.43	5.58	...
S_2-S_1 B_u/A_g MECI	5.79	...	...
S_2-S_1 Me^-/C^* MECI	5.47	...	...
S_2-S_1 Me^+/C^* MECI	5.70	...	...
S_1-S_0 transoid MECI	4.55	4.99	4.57
S_1-S_0 Me^- MECI	4.30	4.47	...
S_1-S_0 Me^+ MECI	4.50	4.84	...

[a]Computed at the BLYP/6-31G ground-state optimized geometry.
[b]Corresponds to a minimum only for in-plane modes.
[c]Computed at the twisted Terminal methylene geometry from Fig. 5(b) ($\theta^{term} = 90°$).

"polyene-like" pathways are involved in the dynamics and to quantitatively predict their branching ratio. Our second goal is to make a direct comparison with the TRPES and TRPEPICO results of Paper I,[14] both to validate the AIMS simulations and also to provide a detailed mechanistic description of the ultrafast dynamics underlying the experimental spectra. It is important to note that in the AIMS simulations of the TRPES spectra, the only adjustable parameters were the ratios of the intensities of one- and two-photon ionization channels.

As presented below, our MSPT2 simulations show excellent agreement with the experimental results and largely support the mechanism deduced previously,[19] albeit with some differences in the branching ratios for different decay pathways. In addition, we confirm the expectation that BD's excited-state dynamics are dictated by the close proximity of the 1^1B_u and 2^1A_g states by constructing two hypothetical scenarios where the electronic structure is biased toward either the bright state or the dark state (i.e., removing their near degeneracy) through a judicious choice of active space and state averaging. Interestingly, we find the excited state lifetime in both the bright-biased and dark-biased simulations to be noticeably extended relative to our reference SA-3-MSPT2 simulations, resulting in qualitative differences in the TRPES observables and a concomitant lack of agreement with experiment.

This paper is organized as follows. In Sec. II, we describe our methods and review the AIMS approach at the MSPT2 electronic structure level of theory. We then describe our approach to simulating TRPES observables and present a method for calculating Dyson orbitals at the MSPT2 level that includes orbital relaxation. We also describe how we assign non-adiabatic transitions in BD using Boys diabatization. In Sec. III, we present our results and compare our simulated TRPES to the experimental results of Paper I,[14] providing assignments and analysis of the mechanism of excited state decay as predicted by AIMS/SA-3-CAS(4/4)-MSPT2. For comparison, we also present the results from the bright-biased and dark-biased simulations mentioned above. Finally, in Sec. IV, we present our conclusions.

II. METHODS

We performed excited-state dynamics of BD using the *Ab Initio* Multiple Spawning[12,25,26] (AIMS) method with the electronic structure calculated using state-averaged complete active space multistate second order perturbation theory[27] (SA-CAS-MSPT2/6-31G**). Analytical gradients[28] and non-adiabatic coupling vectors (NACVs)[12,29] for SA-MSPT2 are available in our locally modified version of Molpro2006.2.[30] This level of theory was previously shown to give an accurate description of the relevant electronic states of BD.[19] A level shift of 0.3 a.u. was used in the MSPT2 calculations. The active space consists of four electrons in four orbitals (4/4) and the averaging spans the three lowest singlet states, i.e., SA-3-CAS(4/4)-MSPT2. With this method, the 1^1B_u and 2^1A_g vertical excitations are 6.35 and 6.47 eV, respectively, in reasonable agreement with the current best theoretical estimates (6.21 ± 0.02 and 6.39 ± 0.07 eV, respectively).[18] This is within the expected accuracy of MSPT2.[31] In addition, we performed minimum energy conical intersection (MECI) optimizations of BD at the MSPT2 level of theory, using analytical gradients[32] and NACVs[12,29] as implemented in the release version of Molpro 2012.1.[33,34] The MECIs are in agreement with those previously published using a penalty-function optimization method.[35] These and other critical points of BD are given in Table I.

The AIMS method has been described in detail elsewhere.[12,25,26,36,37] Briefly, the total molecular wavefunction is decomposed as a product of electronic and nuclear wavefunctions, summed over all electronic states,

$$\Psi(\mathbf{r},\mathbf{R},t) = \sum_I \chi_I(\mathbf{R},t)\phi_I(\mathbf{r};\mathbf{R}), \tag{1}$$

where $\mathbf{r}$ and $\mathbf{R}$ are the electronic and nuclear coordinates, respectively, I is the electronic state label, and $\chi_I(\mathbf{R},t)$ and $\phi_I(\mathbf{r};\mathbf{R})$ are the nuclear and electronic wavefunctions, respectively. The nuclear wavefunction is further expanded as a linear combination of complex frozen Gaussian trajectory basis functions (TBFs),

$$\chi_I(\mathbf{R},t) = \sum_i c_I^i(t)\chi_I^i\left(\mathbf{R},\overline{\mathbf{R}}_I^i(t),\overline{\mathbf{P}}_I^i(t),\gamma_I^i(t);\alpha\right), \tag{2}$$

where i labels the TBF on state I and $c_I^i(t)$, $\overline{\mathbf{R}}_I^i(t)$, $\overline{\mathbf{P}}_I^i(t)$, and $\gamma_I^i(t)$ are the complex amplitude, position, momentum, and phase of the TBF, respectively. The Gaussian width parameters, α, of the TBFs are element specific and have been previously optimized to best represent the ground-state wavefunctions for a variety of molecules.[38] Each TBF evolves independently on the potential energy surface of its associated electronic state according to the classical equations of motion for $\overline{\mathbf{R}}_I^i(t)$ and $\overline{\mathbf{P}}_I^i(t)$, using forces calculated *on-the-fly* from the *ab initio* electronic structure with an adaptive velocity Verlet integrator.[26] The TBF phase $\gamma_I^i(t)$ is propagated semiclassically and $c_I^i(t)$ is determined by solving the time-dependent Schrödinger equation on the basis of TBFs, thereby allowing population transfer between the TBFs.

Having specified the basis and propagation scheme in AIMS, dynamics were then initiated by Monte Carlo sampling $\overline{\mathbf{R}}_I^i(t)$ and $\overline{\mathbf{P}}_I^i(t)$ from the ground-state molecular Wigner distribution in the harmonic limit. Following Ref. 19, for BD, this was accomplished by calculating the vibrational normal modes and frequencies at the BLYP/6-31G level of theory, which gave good agreement with the experimental frequencies.[39] Next, in order to model a pump excitation laser pulse, the initial TBFs were projected onto the excited state of interest under the condition that the energy gap was resonant with the pump laser, following a commonly used mixed/quantum classical procedure.[40,41] First, for each geometry sampled from the ground-state Wigner distribution, the bright state was identified as the vertical adiabatic state with the largest transition dipole to the ground state. Then, if the vertical excitation energy for the state of interest (bright or dark) was within the pump laser energy resonance condition, e.g., 5.74 ± 0.03 eV, trajectories were launched on that state within the independent first generation approximation, i.e., the sampled TBFs

were initially uncoupled and run independently.[36,37] To allow for population transfer between electronic states, AIMS adaptively increases the number of TBF basis functions when regions of large non-adiabatic coupling are encountered in a process called *spawning*. When the non-adiabatic coupling of a parent TBF crosses a threshold value (i.e., in the vicinity of an electronic state crossing), the AIMS code monitors the magnitude of the coupling and places a child TBF on the coupled state at the peak of the coupling. Following semi-classical arguments, the momentum of the child TBF is scaled along the NACV to match the classical energy of the parent. If this scaling is not possible (i.e., there is insufficient kinetic energy along the NACV for an upward electronic transition), spawning is aborted in a manner similar to the treatment of frustrated hops in surface hopping.[42] Finally, to ensure that the child TBF can be initiated with zero amplitude, it is back propagated and added to the basis before the coupling region is entered.

The simulation time step was chosen to be 10 a.u. but was allowed to adaptively decrease to as little as 0.1 a.u. in the vicinity of a conical intersection in order to adequately sample the rapidly changing NACV. Spawning was initiated when the magnitude of the NACV reached 10 a.u. but was suppressed if the nuclear Mulliken population[43,44] of the parent was less than 1% or if another TBF on the coupled state was nearly redundant with the parent (defined by a nuclear overlap matrix element with an absolute value exceeding 0.6). Due to the high computational cost of MSPT2 electronic structure calculations and to allow the simulations to be run for 500 fs and longer, we stopped TBFs that were spawned on S_0 after they remained uncoupled (with a maximum overlap $|S| < e^{-10}$) from other trajectories for 5 fs, a period long enough for the ground-state trajectories to leave the coupling region. These trajectories were then restarted with the computationally less expensive state-specific SA-3-CAS(4,4)-SSPT2 method. This amounts to neglecting off-diagonal elements of the MSPT2 effective Hamiltonian,[27] which is a very good approximation for the ground state away from a conical intersection. Nevertheless, the zeroth-order Fock matrix of SSPT2 differs from that of MSPT2 due to a lack of state averaging; thus, the S_0 PES (and to a lesser degree its first derivative) is discontinuous at the point of switching between MSPT2 and SSPT2. As a result of this procedure, the S_0 trajectories are continuous but not differentiable at the restart point. We verified that this did not introduce severe artifacts by monitoring the classical kinetic energy of the restarted trajectories and saw no noticeable heating of the system, indicating that the gradients of SS-CASPT2 closely matched those of SA-3-CAS(4/4)-MSPT2 at the restart points.

As described in the Introduction, we performed three sets of AIMS simulations on BD. In "Simulation 1," we modeled a 1-photon excitation of BD by initiating trajectories on the dipole-allowed 1^1B_u state at the SA-3-CAS(4/4)-MSPT2 level of theory. This level of theory provides a balanced description of both the 1^1B_u and 2^1A_g excited states and will be considered our "reference" and the best prediction available. We modeled the experimental pump photon energy of 5.74 ± 0.03 eV (216 nm) by selecting only initial conditions that had an excitation energy to the bright state within this range. The bright state was identified based on the magnitude of the transition dipole moment connecting it to the ground state. In some instances, both S_1 and S_2 had appreciable transition dipole moments due to the energetic proximity of these states, so we followed the procedure of Ref. 19 and selected the state with the largest transition moment. A more accurate approach would form a coherent superposition of two TBFs, one on each state, with nuclear wavefunction amplitudes maximizing the resulting transition dipole moment. There was no reason to pursue this more complicated approach here because none of the 25 initial conditions had both electronic states simultaneously within the pump excitation energy window. Our method of preparing the initial conditions is shown schematically in Fig. 2 which plots the relevant potential energy surfaces and ground and excited state wavepacket distributions along the bond-alternation (BA) coordinate, defined in Fig. 2. Since the pump energy is to the red of the vertical excitation energy, the excitation is closer to adiabatic in character and the initial wavepacket distribution is displaced significantly along the BA coordinate and to a lesser extent along other modes which are coupled to the ground-excited energy gap.

As shown in Fig. 2, the BA coordinate also strongly modulates the 1^1B_u-2^1A_g energy gap, bringing about a crossing at ΔR = 0.08 Å. In fact, for the majority (80%) of initial conditions, the 1^1B_u state is S_2, i.e., the reverse of the state ordering at the FC point. Nevertheless, 1^1B_u and 2^1A_g were still initially close in energy and, therefore, the results are comparable to the previous AIMS simulations on BD[19] which assumed a vertical excitation. For "Simulation 1," 25 initial conditions were chosen and these spawned a total of 298 additional TBFs.

As discussed below, another important geometry to consider besides the planar FC region is the fully twisted geometry

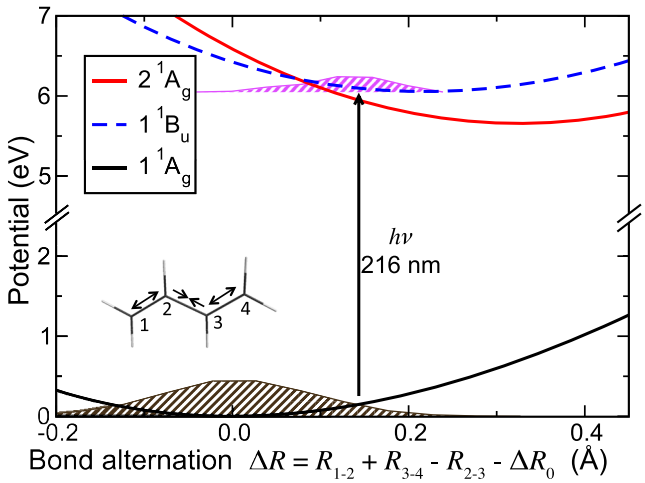

FIG. 2. Potential energy curves and ground- and excited-state wavepacket distributions of BD along the bond alternation (BA) coordinate, defined on the abscissa, where $R_{i\text{-}j}$ is the carbon i-carbon j bond length (atom labels defined in the figure inset) and ΔR_0 is the ground-state equilibrium value of the BA coordinate (ΔR_0 = 1.25 Å). The potentials were calculated at the SA-3-CAS(4/4)-MSPT2/6-31G** level of theory with a level shift of 0.3 a.u., with equal displacements in $R_{1\text{-}2}$, $R_{3\text{-}4}$ and $R_{2\text{-}3}$. The vibrational wavepacket densities were generated by Monte Carlo sampling of the ground-state Wigner distribution and projecting on the BA coordinate. The BA coordinate strongly modulates the energy gap between the 1^1B_u and 2^1A_g states such that they exhibit a diabatic crossing at ΔR = 0.08 Å, close to the FC geometry. Adiabatic excitations to the planar minimum of the 1^1B_u state therefore have the dark state *below* the bright state, the reverse order of that for a vertical excitation.

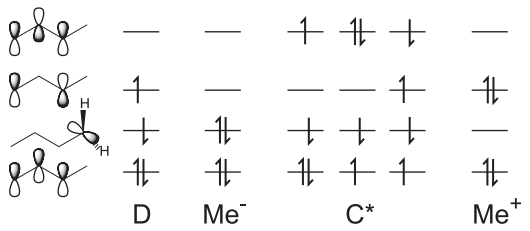

FIG. 3. Electronic structure of BD under C_s symmetry (twisted terminal methylene), showing qualitatively the π molecular orbitals and the predominant electron configurations for the lowest four electronic states. D is the fully twisted ground state diradical; C^* is a covalent state involving significant configuration mixing; Me^- and Me^+ are two charge transfer (CT) states with the terminal *p* orbital doubly occupied and unoccupied, respectively.

of C_s symmetry. At this geometry, the terminal carbon *p* orbital is uncoupled from the remaining π system, resulting in an electronic structure that is shown qualitatively by the orbital occupations in Fig. 3.[9] The fully twisted ground state is diradical (D), while the lowest three excited states are a covalent state (C^*) involving significant configuration mixing, and two charge transfer (CT) states (Me^- and Me^+) with the terminal *p* orbital doubly occupied and unoccupied, respectively. The energies of the C^* and Me^- states calculated at the reference SA-3-CAS(4/4)-MSPT2 level of theory are presented in Table I. It can be seen that these states are very close in energy, suggesting both will be important in BD excited state dynamics.

In the second set of simulations, we modified the electronic structure to bias the bright ^1B_u state of BD by using an active space of 2 electrons in 2 orbitals, averaged over the lowest two singlet states: SA-2-CAS(2/2)-MSPT2. The effect of this reduced active space can be understood by considering Fig. 1: by removing the HOMO−1 and LUMO+1 orbitals from the active space, the configuration mixing in the 2^1A_g state is removed at the CASSCF level (the zeroth order reference on which MSPT2 is based), raising the energy of this state significantly, while leaving the 1^1B_u state largely unchanged. In the same way, Fig. 3 shows that at this level of theory, the C^* state is also penalized, while leaving the Me^- and Me^+ states intact (see Table I). The 2^1A_g and C^* states are not completely removed, however, and geometric distortions away from C_{2h} or C_s symmetries may give rise to a mixing-in of their character on the S_1 state. Indeed, as shown in Table I, the dark-character transoid S_1-S_0 MECI still exists at this "bright-biased" level of theory, although shifted to a somewhat higher energy.

The dynamics simulation protocol for the bright-biased trajectories was unchanged from Simulation 1, aside from sampling initial conditions with an excitation energy of 5.84 ± 0.03 eV [to correct for the slightly larger 1^1B_u vertical excitation energy at the SA-2-CAS(2/2)-MSPT2 level of theory]. Here 25 initial trajectories were run and these spawned 125 additional TBFs.

Finally, in the third set of simulations, we modified the electronic structure to bias in favor of the BD dark state. This was achieved by taking advantage of the excessively large excitation energy of the bright 1^1B_u state at the CASSCF level of theory and performing a 2-state averaged calculation that included only the ground and dark 2^1A_g state. This procedure ensured that the S_1 state remained dark for the duration of the dynamics at the SA-2-CAS(4/4)-MSPT2 level of theory. In addition, the Me^- and Me^+ states were removed, since at C_s symmetry these are S_2 and S_3 at the CASSCF level. Encouragingly, as shown in Table I, the quality of the dark state description was not impacted by modifying the electronic structure in this way: the 2^1A_g vertical and adiabatic excitations and dark transoid conical intersection energies were within 0.02 eV of the SA-3-CAS(4/4)-MSPT2 values. However, the charge-transfer intersections, Me^- and Me^+, are no longer intersections, and an MECI optimization starting from these geometries converged to the transoid MECI.

The dynamics simulation protocol for the dark-biased trajectories was again unchanged from Simulation 1, except here we initiated trajectories directly on the 2^1A_g state. This procedure may thus be understood as assuming a near-instantaneous non-adiabatic transition from the 1^1B_u state to the 2^1A_g state or alternatively a 2-photon excitation (432 nm × 2) directly to the 2^1A_g state. Here 25 initial trajectories were run on the 2^1A_g state and these spawned 61 additional TBFs. Interestingly, we note that, experimentally, the dark 2^1A_g state directly populated by two-photon excitation at 400 nm has a longer phenomenological lifetime than does one photon excitation at 200 nm of the 1^1B_u state.[45,46]

In order to make a direct connection between our simulated results and experimental observables, we used a recently developed framework to calculate TRPES from the AIMS trajectories. As the details of our TRPES framework are described elsewhere,[12,13,23,47] we include here only a brief outline in order to describe our choice of parameters and implementation details for the specific case of BD.

The starting point for our TRPES framework is the photoionization matrix element that connects an initial *N*-electron neutral state with a final state consisting of an $(N-1)$-electron cation state and a continuum electron. Within the sudden approximation,[48,49] correlation between the cation and continuum electron is taken to be negligible, allowing the final state to be represented as a direct product of the cation and continuum wavefunctions. Within the dipole approximation, the electronic part of the photoionization matrix element is

$$\begin{aligned} D_{I,F\eta} &= \left\langle \phi_I^N(\mathbf{r}_1,\ldots,\mathbf{r}_N)\right| \hat{\mu}(\mathbf{r}_1,\ldots,\mathbf{r}_N)\left|\phi_F^{N-1}(\mathbf{r}_2,\ldots,\mathbf{r}_N)\phi_\eta^{el}(\mathbf{r}_1)\right\rangle \\ &\approx \left\langle \varphi_{IF}^D(\mathbf{r}_1)\right| \hat{\mu}(\mathbf{r}_1)\left|\phi_\eta^{el}(\mathbf{r}_1)\right\rangle, \end{aligned} \tag{3}$$

where the second equality results from the strong orthogonality condition between the cation and continuum electron.[50] The index η is a composite index of the quantum state of the continuum electron (i.e., specifying energy and angular momentum), and the Dyson orbital φ_{IF}^D is given by the overlap of neutral and cationic states,

$$\left\langle \varphi^D_{IF}(\mathbf{r}_1)\right| = \sqrt{N}\left\langle \phi^N_I(\mathbf{r}_1,\ldots,\mathbf{r}_N)\right|\left.\phi^{N-1}_F(\mathbf{r}_2,\ldots,\mathbf{r}_N)\right\rangle_{\mathbf{r}_2,\ldots,\mathbf{r}_N}, \tag{4}$$

where the integration is over all electronic coordinates except for those of the ejected photoelectron, $\mathbf{r}_1$. The advantage of Eq. (4) is that it allows the photoionization matrix element to be calculated from a simple 3D integral, provided that the Dyson orbital and continuum wavefunctions are known. Below, we describe how to extract Dyson orbitals from MSPT2 electronic structure calculations. Finally, we work in the limit that the continuum electron interacts with the ionized molecule only through its point charge potential such that the continuum functions correspond to Coulomb partial waves. Equation (3) is then evaluated on a 3D grid using the ezDyson v2 code, which includes angular averaging of the photoionization matrix element.[51,52] For BD, we found that converged photoionization matrix elements were obtained by including partial waves up to $l = 5$ and using a quadrature grid of $128 \times 128 \times 128$ points with a length of 10 Å on each side.

With this formalism for calculating photoionization matrix elements for particular nuclear configurations, we then followed a semi-classical prescription and defined the total time-resolved photoelectron spectrum (a function of electron kinetic energy E_k and time t) as an incoherent sum of the contributions from each TBF (with the matrix element evaluated at its centroid), weighted by their nuclear populations $n^I_i(t)$,

$$P(E_k,t) \propto \frac{\omega_{probe}}{k}\sum_{I,i,F,\eta} n^I_i(t)\left|D_{I,F\eta}\left(\bar{R}^I_i\right)\right|^2 \times \delta\left(\hbar\omega_{\text{probe}} - IP_{I-F}\left(\bar{R}^I_i(t)\right) - E_k(\eta)\right). \tag{5}$$

The delta function in Eq. (5) ensures energy conservation between the probe pulse ($\hbar\omega$) and the final ionization continuum state (i.e., the sum of the instantaneous ionization potential $IP_{\text{I-F}}$ and excess electron kinetic energy E_k). For BD, we included $S_0/S_1/S_2$ in the sum over neutral states and D_0/D_1 in the sum over cationic states. The cation states were evaluated using SA-2-CAS(3/4)-MSPT2/6-31G** with a level shift of 0.3 a.u. To correct for any deficiencies in the calculated ionization potentials at the MSPT2 level, we applied a uniform shift of +0.7 eV to the cation state energies relative to the neutral states—this shift brings the simulated early time TRPES in line with experiment. Finally, to match the experimental energy and time resolution (Paper I[14]), we convolved Eq. (5) with a temporal Gaussian of 160 fs full width at half maximum (FWHM) and an energy-domain Gaussian of 0.15 eV FWHM.

We previously showed how to generate Dyson orbitals from CASSCF and MSPT2 wavefunctions under the condition that the molecular orbitals in the cation calculation were frozen from the neutral calculation.[11,12,47] In the following, we extend this approach so as to include orbital relaxation in the cation.

The starting point is the second quantized expression for the Dyson orbital,

$$\varphi^D_{IF}(\mathbf{r}) = \sum_k \left\langle \phi^{N-1}_F\right| a_k \left|\phi^N_I\right\rangle \varphi_k(\mathbf{r}), \tag{6}$$

where φ_k is a molecular orbital. Introducing a "null" orbital, φ_0, which represents an idealized zero kinetic energy electron infinitely far from the molecule, the Dyson orbital becomes

$$\varphi^D_{IF}(\mathbf{r}) = \sum_k \left\langle \phi^{N-1}_F\varphi_0\right| a^\dagger_0 a_k \left|\phi^N_I\right\rangle \varphi_k(\mathbf{r}), \tag{7}$$

where the bra state is chosen to have the same spin multiplicity as the ket state. Equation (7) is readily evaluated with existing electronic structure codes. If the bra and ket states are represented using different sets of orbitals (e.g., they come from separately optimized CASSCF calculations), the orbital sets should be bi-orthogonalized and Eq. (7) is modified to read[53]

$$\varphi^D_{IF}(\mathbf{r}) = \sum_k \left\langle \tilde{\phi}^{N-1}_F\tilde{\varphi}_0\right| a^\dagger_0\tilde{a}_k \left|\phi^N_I\right\rangle \varphi_k(\mathbf{r}), \tag{8}$$

where the tilde symbols indicate a state or operator in terms of the bra orbital basis. The weight of molecular orbital k in Eq. (8) can be identified as the 0, k element of the transition density matrix connecting the initial N-electron state and the product of an $N-1$ electron state and a singly occupied null orbital in a bi-orthogonal basis[53] and is thus straightforward to extract from a CI calculation. Following Ref. 27, we take the CI vectors of the MSPT2 states to be the rotated zeroth-order (CASSCF) state vectors,

$$\left|\phi^{\text{MSPT2}}_I\right\rangle = \sum_j c^I_j \left|\phi^0_j\right\rangle, \tag{9}$$

where c^I are the MSPT2 mixing coefficients for state I. In addition, we approximate the null orbital as a single s-type primitive Gaussian orbital with exponent 1×10^{-12} centered 8.7×10^6 bohrs from the molecule.[54] Given its extreme diffuseness and displacement from the molecule, this orbital has an energy of approximately zero and is effectively uncoupled from the remaining CASSCF molecular orbitals. We restrict the null orbital to be unoccupied in the N-electron state and singly occupied in the $N-1$ state. We then use Molpro's CI program to calculate the transition density matrix with bi-orthogonalization in Eq. (8).[30] In the supplementary material, we provide an example Molpro input deck for calculating the Dyson orbital between two CASSCF states.

The formalism for calculating photoionization matrix elements described above is appropriate only for single-photon ionization. As described in Paper I,[14] the two-photon ionization channels involve intermediate excitations to high Rydberg states,[14] which our electronic structure cannot capture. Therefore, we simulated BD ionization resulting from a two-photon probe (denoted as $1 + 2'$ to signify the one-photon pump followed by a differently colored two-photon probe) within the Condon approximation, assuming the two-photon ionization matrix element to be independent of nuclear geometry and empirically adjusted the magnitudes of the spectra in the ratios 900:58:17 for 1-photon:2-photon-S_1:2-photon-S_0 to best match the experimental signal. In this way, the simulated ($1 + 2'$) TRPES spectrum simply reflects changes in the ionization potential and state populations. Despite the Condon approximation, the 2-photon contribution to the total simulated TRPES spectrum in Fig. 4(b) agrees very well with the experimental result of Fig. 4(a) (discussed in detail below).

In order to obtain branching ratios for BD excited state dynamics, we needed a means to characterize the various conical intersections visited during dynamics. The usual

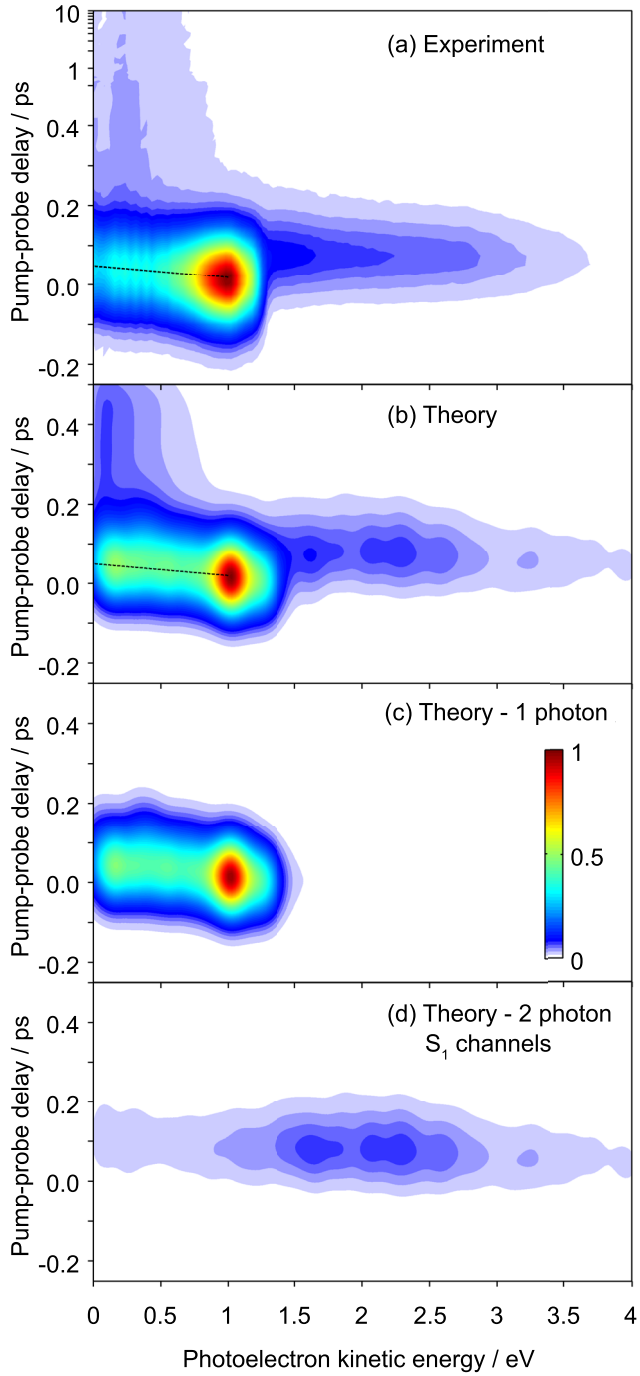

FIG. 4. Experimental and simulated time-resolved photoelectron spectra of BD for 216 nm pump and 267 nm probe wavelengths. Panel (a) replots the experimental TRPES result from Fig. 8(a) of Paper I.[14] The dotted black line emphasizes the shift of the most probable photoelectron kinetic energy with time. Note that the y axis is shown on a logarithmic scale after 0.5 ps so that the long-time component in the TRPES can be displayed. Panel (b) shows the simulated total, i.e., (1 + 1′) and (1 + 2′), TRPES spectrum from AIMS simulations, calculated using the formalism of Sec. II with SA-3-CAS(4/4)-MSPT2. The total TRPES spectrum of (b) is resolved into (1 + 1′) contributions shown in panel (c), and the S1 contribution to (1 + 2′) is shown in panel (d). The long-time component in the TRPES seen in panels (a) and (b) originates from 2-photon ionization of the "hot" S_0 ground state.

approach[12,23] of labeling a spawning geometry according to the nearest MECI (smallest root mean squared displacement) was unsatisfactory in BD. This is because BD has multiple energetically accessible CIs that are geometrically quite similar (see below). Thus, rather than relying on the nuclear geometry alone to characterize a non-adiabatic transition, we also consider the electronic wavefunction at each spawn event. In particular, we distinguish Me^-, Me^+, and covalent states by the Mulliken charges on the BD terminal methylene units. One caveat with this approach is that the adiabatic electronic states of a molecule near a conical intersection are in general of rapidly varying mixed character. To overcome this problem, we constructed approximate diabatic states according to Subotnik's Boys localization procedure (closely related to the Mulliken-Hush procedure[55] for a two-level system). After finding the adiabatic-to-diabatic rotation angle $\theta^{\text{a-d}}$, diabatic density matrices ρ^{d} were constructed according to

$$\begin{aligned}\rho_0^{\text{d}} &= \cos^2(\theta^{\text{a-d}})\rho_{i,i}^{\text{a}} + 2\sin(\theta^{\text{a-d}})\cos(\theta^{\text{a-d}})\Re e(\rho_{i,j}^{\text{a}}) \\ &\quad + \sin^2(\theta^{\text{a-d}})\rho_{j,j}^{\text{a}}, \\ \rho_1^{\text{d}} &= \sin^2(\theta^{\text{a-d}})\rho_{i,i}^{\text{a}} - 2\sin(\theta^{\text{a-d}})\cos(\theta^{\text{a-d}})\Re e(\rho_{i,j}^{\text{a}}) \\ &\quad + \cos^2(\theta^{\text{a-d}})\rho_{j,j}^{\text{a}},\end{aligned} \tag{10}$$

where $\rho_{i,j}^{\text{a}}$ is a (transition) density matrix for adiabatic states i (and j). We then performed Mulliken population analysis on the diabatic density matrices and defined a state as CT-like when a terminal methylene unit (CH_2) had a charge of at least 0.45 e in magnitude.

In addition to labeling the electronic character of each non-adiabatic transition, we also monitored the central C–C bond torsion angle (using the coordinate system described in the supplementary material) and labeled transitions as *trans*: $150° < |\theta| \leq 180°$, *transoid*: $90° < |\theta| \leq 150°$, or *cisoid*: $30° < |\theta| \leq 90°$.

III. RESULTS AND DISCUSSION

We consider first the experimental TRPES spectrum of BD for 216-nm pump and 267-nm probe wavelengths from Fig. 8(a) of Paper I,[14] replotted here in Fig. 4(a). At small pump-probe time delays, the TRPES reflects photoionization of the initially created wavepacket on the 1^1B_u bright state and its ensuing dynamics. As discussed in detail in Paper I,[14] both one-photon ionization (denoted as 1 + 1′) and two-photon ionization (denoted as 1 + 2′) signals were observed. With the given pump and probe wavelengths, single photon photoionization (1 + 1′) is allowed and dominant for photoelectron kinetic energies below 1.3 eV. Signals with higher photoelectron kinetic energies (>1.3 eV) can only arise from two-photon ionization (1 + 2′). At increasing pump-probe time delays, up to ~50 fs, we see the peak intensity of the photoelectron signal shift to lower electron kinetic energies at a rate of ~40 meV/fs, implying that the instantaneous vertical ionization potential of the 1^1B_u state increases at this rate during the early time dynamics. This "sweep" of the photoelectron kinetic energy is discussed in detail in Paper I.[14]

The experimental and SA-3-CAS(4/4)-MSPT2 AIMS-predicted TRPES are shown in Figs. 4(a) and 4(b), respectively. Excellent agreement is obtained with no adjustable parameters other than the ratio of intensities of the 1- and 2-photon photoionization channels. This gives us confidence that AIMS with the reference SA-3-CAS(4/4)-MSPT2 electronic structure method provides a faithful representation of

BD excited state dynamics. In the following, we analyze the components of the simulated spectrum and assign the features of the experimental TRPES.

We start by considering the simulated (1 + 1′) TRPES, plotted in Fig. 4(c). As discussed in terms of Koopmans' correlations in Paper I,[14] this is dominated by the S_2-D_0 photoionization channel, with a small contribution from the S_1-D_0 channel when S_1 has bright character. The simulated (1 + 1′) TRPES is in remarkable agreement with the early time experimental TRPES spectrum. In particular, the spectrum initially peaks at ∼1 eV and rapidly shifts to lower electron kinetic energy at a rate of about −40 meV/fs, matching the experimental behavior presented in Paper I.[14]

An understanding of the molecular motions that give rise to such a large and rapid increase in the 1^1B_u ionization potential during the first 30 fs of dynamics would provide a crucial link between the photoelectron observables and the mechanism of non-radiative decay in BD. On examining the excited-state trajectories, we found that a twisting motion around a single terminal C–C bond [see the inset of Fig. 5(b)] had sufficiently large amplitude motion on the 30-fs time scale to increase the excited-state ionization potential by 1 eV. This is presented in Fig. 5(a), which shows the S_2 excited-state wavepacket density projected onto the maximally twisted terminal torsion coordinate, θ^{term}, using the Monte Carlo analysis method of Ref. 56. During the first 30 fs after photoexcitation, the wavepacket center moves to a twist angle of $\theta^{\text{term}} \sim 55°$, while the wavepacket dispersion along this coordinate remains roughly constant. After this initial motion, the S_2 wave-packet then bifurcates, with roughly half of the population continuing to twist to $\theta^{\text{term}} \sim 100°$ and then decaying to S_1, while the remaining population oscillates around $\theta^{\text{term}} \sim 50°$, while decaying to S_1.

The initial terminal twisting motion of BD on its ^1B_u state is indeed connected to a large increase in ionization potential, as demonstrated in Fig. 5(b), which plots the excited-state potential energies along θ^{term}, while optimizing all in-plane modes on the S_2 state (whose higher frequencies adiabatically separate them from the terminal twist motion).[57] A terminal twist of zero degrees in this figure corresponds to the BD ^1B_u planar-constrained minimum geometry of C_{2h} symmetry; thus, according to Fig. 2, S_2 is the bright state. With increasing twist angle, the potential energy of S_2 is lowered toward a minimum at $\theta^{\text{term}} \sim 50°$, followed by a barrier at $\theta^{\text{term}} \sim 70°$, thus explaining the initial wave-packet dynamics and bifurcation seen in Fig. 5(a). In concert with this, the potential energy of the D_0 state rises with increasing twist angle such that the ionization potential of the ^1B_u state increases from 3.36 eV at $\theta^{\text{term}} = 0°$ to 4.30 eV at $\theta^{\text{term}} = 55°$, explaining the observed ∼1-eV red-shift in the photoelectron peak during the first 30 fs of dynamics. At twist angles greater than 80°, the ionization potential of S_2 exceeds the probe photon energy which, together with S_2-S_1 internal conversion, leads to a rapid disappearance of the (1 + 1′) TRPES signal. Finally, at the fully twisted geometry, $\theta^{\text{term}} = 90°$, the molecule has C_s symmetry and, following Sec. II, the adiabatic states are $S_1 = Me^-$, $S_2 = C^*$ with a small splitting of 0.06 eV.

In addition to explaining the observed red-shift in the photoelectron signal, the plot of the BD potential energy curves along the terminal twist coordinate, shown in Fig. 5(b), also points to the mechanism of the S_2-S_1 non-adiabatic transition: the S_2-S_1 energy gap decreases from 0.33 eV at $\theta^{\text{term}} = 0°$ to 0.11 eV at $\theta^{\text{term}} = 55°$. This suggests that a nearby conical intersection would make electronic transitions particularly efficient at terminally twisted geometries. Indeed, a MECI optimization, starting from the $\theta^{\text{term}} = 55°$ geometry and relaxing all

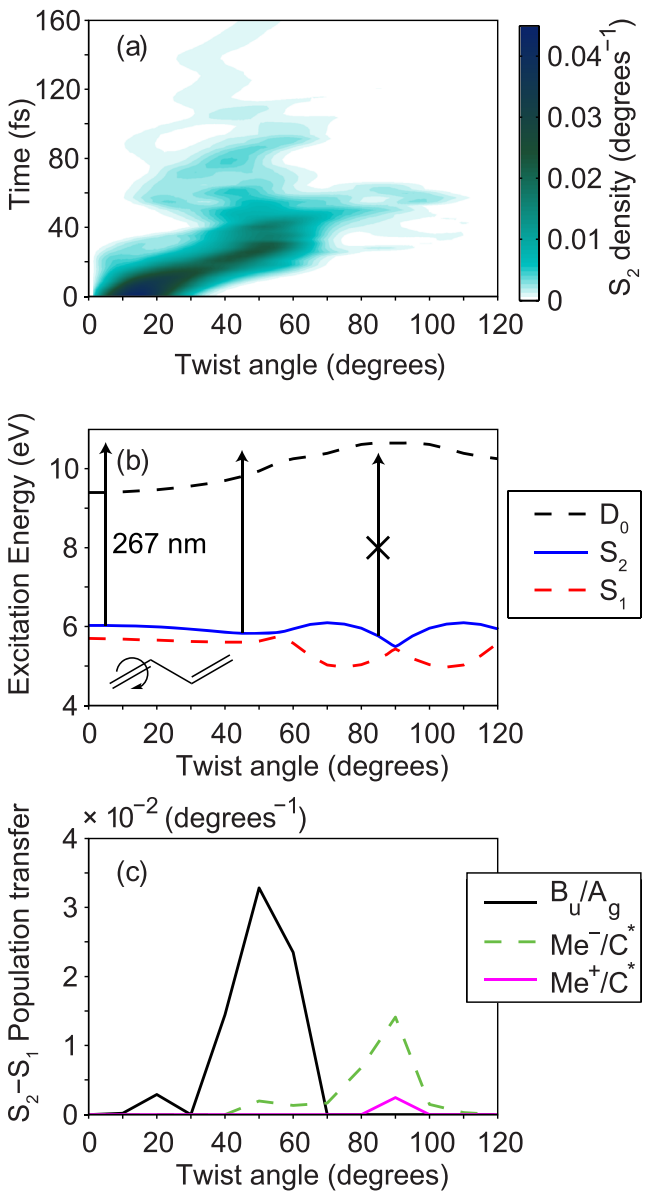

FIG. 5. Terminal twisting dynamics of BD on S_2. Panel (a) shows the projection of the S_2 wavepacket density on the maximally twisted terminal torsion coordinate [indicated in panel (b)], calculated using a Monte Carlo method.[56] Panel (b) plots the S_2 potential energy curve (solid blue) along the terminal twist coordinate with in-plane modes optimized on S_2 and all other out-of-plane modes frozen. S_1 and D_0 energies (after applying an empirical +0.7 eV shift to D_0) are shown with dashed red and black lines, respectively. Vertical arrows indicate the energetic accessibility of D_0 from S_2 with a 267-nm probe pulse. Panel (c) plots the average absolute S_2-S_1 population transfer versus maximal terminal twist angle at the spawning geometry for three classes of S_2-S_1 conical intersections. The peak in the B_u/A_g population transfer (solid black line) coincides with an MECI between these states with $\theta^{\text{term}} = 52.3°$ [see Fig. 6(a)]. At twist angles close to $\theta^{\text{term}} = 90°$, the Me^-/C^* and Me^+/C^* charge-transfer/valence conical intersections dominate the population transfer (dashed green and solid magenta lines, respectively), with the relevant MECIs shown in Figs. 6(b) and 6(c).

degrees of freedom, converged on a S_2-S_1 MECI, depicted as the "B_u-A_g MECI" in Fig. 6(a), with a terminal twist of $\theta^{term} = 52.3°$. Furthermore, in our spawning simulations, the dominant S_2-S_1 population transfer occurred for θ^{term} between 50° and 60°, which is shown in Fig. 5(c) as a distribution of the population transfer from S_2 to S_1 during spawning versus the maximal terminal twist angle at the spawning event. A Mulliken population analysis of the electronic states involved in the spawning events with $50° < \theta^{term} < 60°$ revealed they were predominantly covalent in nature, consistent with our assignment of a B_u-A_g MECI. It should be noted, however, that the S_2-S_1 non-adiabatic transition does not occur solely at these twist angles: spawning geometries with $\theta^{term} \sim 90°$ also contribute significantly to the population transfer. As Fig. 5(b) suggests, this is due to the presence of S_2-S_1 conical intersections between the CT and covalent states at fully twisted geometries, such as the Me^-–C^* MECI depicted in Fig. 6(b) which corresponds to the lowest energy S_2-S_1 CI (see Table I).

The features of the potential energy surfaces in Fig. 5(b) are consistent with the extrapolated MRCI results of Bonacic-Koutecky *et al.*,[9] implying that the barrier on S_2 results from an avoided crossing between S_2 and S_3, with the upper state being predominantly Me^+ in character at terminally twisted geometries. Although our choice of three-state averaging precludes a simultaneous description of the ground, C^*, Me^-, and Me^+ states, it is evident that the influence of the Me^+ state is seen in features of the S_2 potential energy surface. Furthermore, geometric distortions away from C_s symmetry can lower the energy of the Me^+ state such that it becomes S_2 or even S_1. This is confirmed in our simulations by the observation of some fraction of S_2-S_1 population transfer proceeding via a Me^+–C^* intersection [magenta curve in Fig. 5(c)]. In addition, we were able to locate a S_2-S_1 Me^+–C^* MECI, shown in Fig. 6(c). This figure indicates that pyramidalization on the carbon adjacent to the terminally twisted methylene is responsible for stabilizing the Me^+ state, although, as Table I shows, the energy of the S_2-S_1 Me^+–C^* MECI is 0.23 eV higher than the Me^-–C^* MECI, consistent with the latter being the more dominant channel.

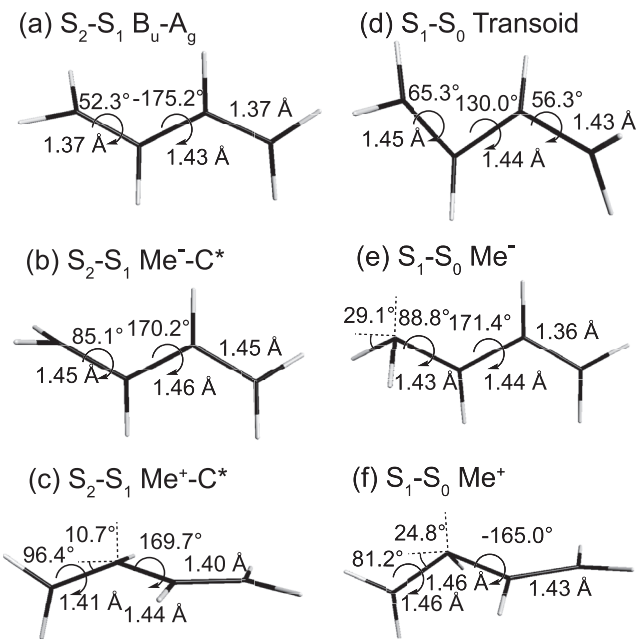

FIG. 6. Geometries of the three S_2-S_1 [(a)–(c)] and three S_1-S_0 [(d)–(f)] minimal energy conical intersections (MECIs) of BD optimized with our reference electronic structure SA-3-CAS(4/4)-MSPT2/6-31G**. Selected pyramidalization angles, C–C torsion angles, and C–C bond lengths are shown.

To summarize, the S_2 excited-state dynamics of BD, probed by (1 + 1′) photoionization, can be understood by the following. In the initial FC region, large amplitude twisting about a single terminal C–C bond gives rise to an increase in the instantaneous vertical ionization potential of the ^1B_u state (primarily due to destabilization of the cation D_0 state) and a concomitant rapid red-shift in the TRPES spectrum, as described in Paper I.[14] The twisting motion also reduces the S_2-S_1 energy gap, leading to non-adiabatic transitions between these states, which become dominant at twist angles between 50° and 60°. Some S_2 population, however, misses the conical intersection at $\theta^{term} = 52.3°$, overcomes a small barrier on S_2, and instead reaches the CT S_2-S_1 CIs at $\theta^{term} \sim 90°$. Although the Me^-–C^* MECI is the lowest energy S_2-S_1 intersection, it is a minor channel because the 1^1B_u-2^1A_g intersection is visited before the CT intersections are reached: a barrier on S_2 separates these regions. The S_2-S_1 non-adiabatic transitions lead ultimately to the disappearance of the (1 + 1′) TRPES signal.

While the (1 + 1′) TRPES spectrum of BD probes mainly the dynamics on the S_2 excited state, the (1 + 2′) process has sufficient energy to access the S_1-D_1, S_1-D_0, and S_0-D_0 ionization channels. In Fig. 4(d), we show the contributions to the (1 + 2′) TRPES arising from the S_1 state alone, which is seen to make up the high-energy tail extending to ~3.7 eV and peaking around a pump-probe time delay of ~80 fs. The good agreement with the measured TRPES data confirms the direct experimental detection of the famously elusive dark 2^1A_g state of BD, as discussed in Paper I.[14] The lack of signals beyond 250 fs in both the (1 + 1′) TRPES and the S_1 part of the (1 + 2′) TRPES [Figs. 4(c) and 4(d), respectively] indicates that the long-time TRPES signal, extending to beyond 0.5 ps [and to beyond 10 ps in the experimental spectrum of Fig. 8(a) of Paper I[14]], comes from 2-photon ionization of vibrationally hot S_0 population. Thus, the decay of the high-energy tail in the 2-photon TRPES arises from the S_1-S_0 non-adiabatic transition which forms the "hot" S_0 ground state, leaving the elusive dark S_1 state of BD with a lifetime of <100 fs.

Given the rather featureless (1 + 2′) TRPES spectrum, there is unfortunately no clear connection between the experimental TRPES and the underlying molecular dynamics involved in the S_1 to S_0 transition. Therefore, in the following, we first focus on the results of the AIMS simulation alone and defer any connections with experimental observables to the end of Sec. III.

As the TRPES spectrum suggests, the lifetimes of both the S_2 and S_1 states of BD are <100 fs. This is shown explicitly in Fig. 7 which plots the population dynamics of the adiabatic states (solid curves) for dynamics initiated on the bright state. To extract lifetimes, we performed an uncertainty-weighted least-squares curve fitting of the combined S_2, S_1, and S_0 populations to a sequential first-order kinetics model over the period $70 < t < 300$ fs.[58] The fit parameters are collected in the first

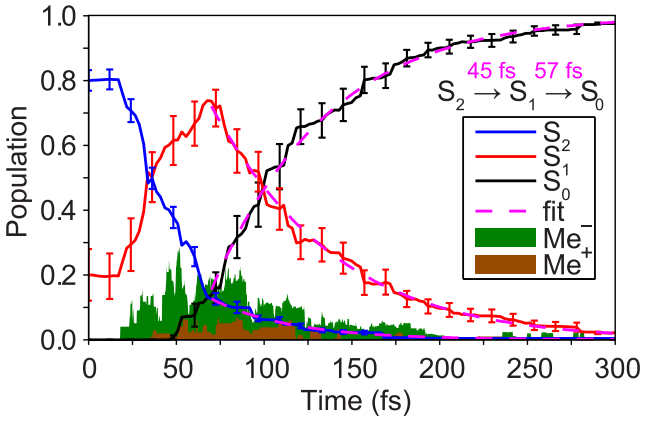

FIG. 7. Adiabatic and charge-transfer population dynamics of BD following 1^1B_u photoexcitation, simulated with AIMS and SA-3-(4/4)-MSPT2. The charge-transfer populations (filled areas) were taken as the incoherent sum of amplitude norms for trajectory basis functions with partial charges meeting the CT definition in Sec. II, summed over all excited adiabatic states. The adiabatic populations (solid curves) are fit to a first-order sequential kinetic model, with the fit shown as the magenta dashed curve and the inverse reaction rate constants shown in the reaction scheme in the inset. Error bars represent 95% confidence intervals calculated by the bootstrap method applied to the population traces from each AIMS initial condition.

column of Table II and the fitted populations, shown as dashed magenta curves in Fig. 7, agree well with the raw population curves.

It is interesting to note the presence of fairly regular, but weak, beat or step patterns in the raw population curves of Fig. 7 (and also Fig. 8). Previous reduced-dimensional models of polyatomic molecular non-adiabatic dynamics also exhibited oscillatory or step patterns in the adiabatic population dynamics that were assigned to coherent vibrational dynamics in the dominant tuning mode(s);[59–62] however, such observations appear not to have been made before in full-dimensional *ab initio* dynamics simulations. It is possible that the beat and step patterns in Figs. 7 and 8, which have a time period of approximately 50 fs, close to the ~700 cm^{-1} CH_2 twist modes of butadiene, arise from coherent vibrational structures. This would certainly be consistent with our proposed mechanism of the terminal CH_2 twist driving the initial S_2 dynamics and leading to the S_2/S_1 non-adiabatic transitions, and there are indeed suggestions of recurrences in the nuclear wavepacket dynamics in Fig. 5. However, we caution against drawing

TABLE II. First-order sequential kinetic model for non-adiabatic population transfer in BD. Parameters are determined from uncertainty-weighted least-squares fits to the population dynamics shown in Figs. 7 and 8.

	Reference	Bright biased	Dark biased
t_0[a]	70 fs	75 fs	100 fs
$P_{S2}(t_0)$[b]	0.1261 ± 0.0067	...	...
$P_{S1}(t_0)$[b]	0.720 ± 0.020	0.4794 ± 0.0087	0.9472 ± 0.0097
$P_{S1}(\infty)$[c]	...	...	0.1546 ± 0.0048
$k_{S2\text{-}S1}^{-1}$	45.4 ± 2.4 fs	...	...
$k_{S1\text{-}S0}^{-1}$	56.75 ± 0.85 fs	126.2 ± 1.8 fs	136.5 ± 3.8 fs

[a] Start time, from which population dynamics are fit.
[b] Initial state populations at start time, t_0. The population of S_0 was constrained to $(1\text{-}P_{S1}\text{-}P_{S2})$.
[c] Long-lived S_1 population. Necessary to fit the population dynamics of the dark-biased trajectories.

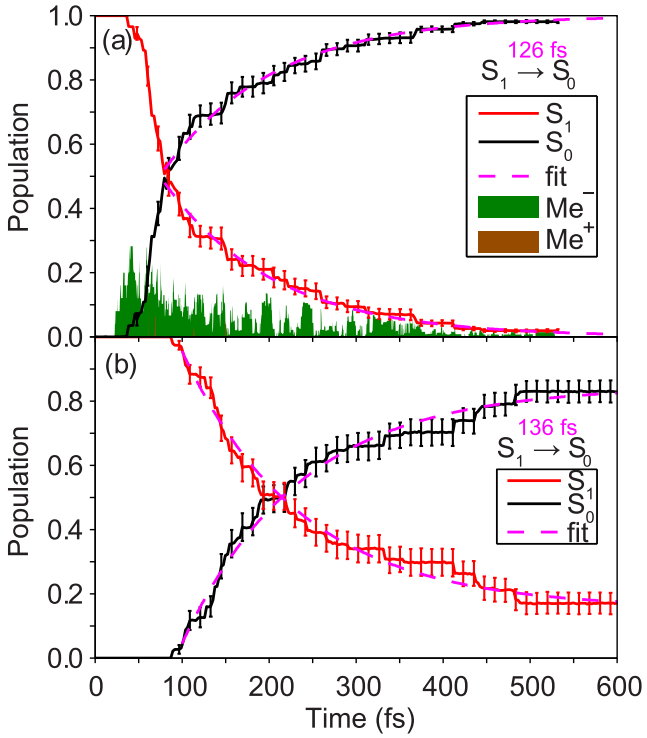

FIG. 8. Excited state AIMS simulation using electronic structure methods biased to include only one bright (a) or dark (b) excited state. Results are plotted following Fig. 7, although with an expanded time axis.

firm conclusions on this from our simulations due to the relatively small number of initial conditions used in this work. For example, step features in the population dynamics could be an artifact of incomplete averaging over vibrational phases due to limited sampling of initial conditions. In this context, we note that AIMS dynamics of ethylene does not exhibit step features in its population dynamics once it is converged with respect to the number of TBFs.[63] Nevertheless, it will be interesting to investigate the robustness of the step structure in the population dynamics for BD once it is possible to extend the simulations to a much larger number of TBFs.

Interestingly, a significant fraction of S_2-S_1 population transfer occurred via CT states (Me^- or Me^+). In order to explore the lifetimes of these states, at each time step, we identified the fraction of excited state trajectories that had CT character (according to the definition in Sec. II) and summed their populations incoherently to give the Me^- and Me^+ populations plotted, respectively, as the filled green and brown curves in Fig. 7. From this figure, it is clear that the CT states persist for the duration of both the S_2 and S_1 lifetimes and, furthermore, the Me^- state is strongly preferred over the Me^+ state, consistent with the branching ratios for the S_2-S_1 Me^-/C^* and Me^+/C^* transitions [Fig. 5(c)].

In order to explore the S_1-S_0 transition in BD in more detail, we analyzed the branching ratios for S_1-S_0 population transfer following the procedure of Sec. II. As shown in Table III, the S_1-S_0 population transfer is spread over several channels: within our statistical uncertainty, the CT intersections and valence intersections (Me^-/trans and neutral/transoid, respectively) are equally important, indicating that both "bright" and "dark" character radiationless decay

TABLE III. Branching ratios for the S_1-S_0 non-adiabatic transition in BD.[a]

Spawn character	Reference (%)	Bright biased (%)	Dark biased (%)
Me^-/trans	26 ± 6	46 ± 9	0
Me^+/trans	11 ± 5	4.0 ± 4	0
Neutral/transoid	23 ± 7	20 ± 7	100
Me^-/transoid	35 ± 9	27 ± 8	0
Me^+/transoid	2.7 ± 2	1.6 ± 2	0
Me^+/cisoid	0.7 ± 0.7	0	0

[a]Uncertainties represent the 95% confidence interval calculated using the bootstrap method.[70]

pathways are operational in BD. Interestingly, we see that as much Me^- S_1-S_0 population transfer occurs with a transoid central C–C torsion as with a trans configuration. Transfer via the Me^+ state is a minor channel, but similar to the Me^- state, it occurs at both trans and transoid central C–C torsions. In addition, a small amount of Me^+ population is transferred at cisoid torsions.

As discussed above, the BD S_2 population is seen to bifurcate into (i) a major channel that undergoes 1^1B_u-2^1A_g non-adiabatic transitions and (ii) a minor channel that reaches CT intersections at fully twisted terminal methylene geometries. An obvious question to ask is whether these S_2 channels give rise to the various S_1 deactivation mechanisms discussed above. To explore this, for each S_2-S_1 transition, we followed the spawned S_1 child trajectory and determined the fraction of its population transferred into the different S_1-S_0 channels during subsequent spawns. Table IV shows the results averaged over all S_2-S_1 transitions. There are clear differences in the subsequent S_1-S_0 branching ratios for the three types of S_2-S_1 transition. For trajectories created by a S_2-S_1 B_u-A_g transition (69% of the S_2 population), the S_1 population is roughly equally split between Me^-/trans, Me^-/transoid, and neut/transoid pathways, with the Me^+/trans and Me^+/transoid being minor channels. On the other hand, for S_2-S_1 Me^-/C^* initiated pathways (28% of the S_2 population), the S_1-S_0 neut/transoid channel is noticeably suppressed, with Me^-/trans and Me^-/transoid being roughly equally more favored. Finally, the minor Me^+–C^* initiated pathway gives rise to more Me^+/trans population than the other S_2-S_1 initiated pathways, although Me^-/transoid appears equally dominant. Thus, our simulations show that the branching ratios for the BD non-adiabatic pathways are to a large extent dictated by the initial dynamics on the ^1B_u state and, in particular, whether the S_2-S_1 non-adiabatic transition occurs at moderately twisted terminal torsion angles (valence intersection) or fully twisted torsions (CT intersections). This finding makes sense in light of the similarity between the S_2-S_1 CT MECI structures and S_1-S_0 MECI structures shown in Fig. 6. In particular, one can see that the Me^- S_1-S_0 intersection can be reached from the Me^- S_2-S_1 intersection simply through pyramidalization of the fully twisted terminal methylene unit. Likewise, the Me^+ S_1-S_0 intersection differs from the Me^+ S_2-S_1 intersection mainly by pyramidalization of the carbon adjacent to the fully twisted methylene.

TABLE IV. Branching ratios for S_1 population resulting from three S_2-S_1 channels.[a]

		S_2-S_1 transition		
		B_u-A_g (%)	Me^-–C^* (%)	Me^+–C^* (%)
S_2-S_0	Relative population	69 ± 8	28 ± 8	2 ± 2
	Me^-/trans	26 ± 9	33 ± 9	7 ± 1
	Me^+/trans	9 ± 6	4 ± 2	39 ± 8
	Neut/transoid	25 ± 9	15 ± 7	8 ± 2
	Me^-/transoid	30 ± 9	44 ± 10	43 ± 9
	Me^+/transoid	6 ± 4	0.0	3 ± 0.6

[a]Determined by labeling each S_1-S_0 and parent S_2-S_1 spawn event according to the procedure described at the end of Sec. II and calculating the S_1-S_0 population transfer relative to the S_1 trajectory's initial population, averaged over all S_2-S_1 spawns. The 5 initial conditions which started on S_1 were not included in this analysis.

Despite the correlation observed between the S_2-S_1 channel and S_1-S_0 channel, it should be noted that our analysis is somewhat simplified. Namely, as mentioned above, a large fraction of non-adiabatic transitions occur at geometries with both CT character and transoid central bond torsion. This finding suggests that a continuous S_1-S_0 CI seam connects the valence and CT MECIs and, furthermore, intermediate points on this seam are energetically accessible upon photoexcitation with a 5.75 eV photon. Thus, although we have partitioned the S_1-S_0 population transfer into the discrete channels listed in Tables III and IV, a more accurate description recognizes that the non-adiabatic transition occurs through a spectrum of distorted structures between Me^-, transoid, and Me^+.

To summarize, the S_2-S_1 and S_1-S_0 deactivation of BD occurs in a sequential manner with time scales of 45 fs and 57 fs, respectively. This is comparable to the experimental 2D global fitting results of 23 fs and 42 fs, respectively, from Paper I.[14] Given the approximations inherent to 2D global fitting, as discussed in detail in Paper I,[14] we consider this agreement to be good. The S_1-S_0 population decay is spread over three classes of CI: (i) a valence transoid intersection; (ii) a Me^- CT intersection; and (iii) a Me^+ CT intersection. The (i) transoid and (ii) Me^- CT intersection pathways were roughly equally dominant in the excited state dynamics. The branching ratios for these intersections are to a large extent governed by initial dynamics on the S_2 state: trajectories passing through S_2-S_1 CT intersections at fully twisted terminal methylene geometries tend to subsequently pass through S_1-S_0 CT intersections.

Having analyzed the excited-state dynamics of BD calculated with our reference SA-3-CAS(4/4)-MSPT2 electronic structure, we now explore the sensitivity of the BD non-adiabatic dynamics to the energetic ordering of its bright 1^1B_u and dark 2^1A_g states. As discussed in Sec. II, we performed two additional sets of AIMS simulations with an electronic structure biased either to the bright state [Simulation 2: SA-2-CAS(2/2)-MSPT2] or to the dark state [Simulation 3: SA-2-CAS(4/4)-MSPT2]. Since each of these calculations invokes two-state averaging, S_1 is the only excited state considered. In the case of the bright-biased SA-2-CAS(2/2)-MSPT2 electronic structure, S_1 has bright character for much of the dynamics. As the second column of Table III shows, a larger fraction of population decays via the (ii) Me^- CT MECIs compared to the reference electronic structure method. This is consistent with a bias against the dark state. However, the dark state is not completely removed and S_1 can adiabatically

become dark in character. This is evidenced by the transoid S_1-S_0 MECI found at this level of theory (see Table I), albeit raised 0.44 eV relative to the transoid S_1-S_0 MECI in the reference electronic structure method. In the case of the dark-biased SA-2-CAS(4/4)-MSPT2 electronic structure, however, S_1 is exclusively dark and, as the third column of Table III shows, S_1-S_0 population transfer occurs only via the (i) transoid MECI at this level of theory.

In Fig. 8, we show the population dynamics for these biased electronic structure simulations. One immediately observes that the excited state lifetime is considerably longer for the biased calculations as compared to the reference calculations, with the bright-biased lifetime [panel (a)] fit to 126 fs and the dark-biased lifetime [panel (b)] fit to 136 fs. In addition, the onset of the S_1-S_0 non-adiabatic transitions is noticeably delayed in the dark-only simulations (~100 fs) compared to the bright-biased and reference simulations (~50 fs). This arises because the backbone dihedral torsion mode needed to reach the transoid intersection has a much higher reduced mass than the twisting and pyramidalization motions of the terminal methylene that lead to the Me^- intersection.

Figure 8 also reveals that the dark-biased simulations have a long-lived excited-state population of ~15% which remains for the duration of our simulation (600 fs). This long-lived component in the dynamics may be related to an S_1 minimum that we located at 4.68 eV above the ground-state minimum. No such minimum was found at either the reference or the bright-biased level of theory.

Given the significantly lengthened excited state lifetimes of BD at the bright-biased and dark-biased levels of theory, one might expect differences in the TRPES spectrum for these simulations, as compared to the reference electronic structure. To explore this, for each model electronic structure, we calculated the TRPES intensity at 2.5 eV which, as Fig. 4 shows, monitors exclusively the excited S_1 population via a $(1 + 2')$ process. The simulated and experimental photoelectron intensities are shown in Fig. 9, where we see excellent agreement between the experimental and simulated TRPES only for the reference electronic structure. As expected from the population dynamics shown in Fig. 8, the TRPES simulated from the bright- and dark-biased calculations are noticeably longer-lived than the experimental signal, with the dark-biased being the longest lived. In addition, the dark-biased signal has an earlier rise, presumably due to the excited state population being initiated directly on the dark S_1 state for these sets of simulations, thereby omitting the bright-dark state transition time scale.

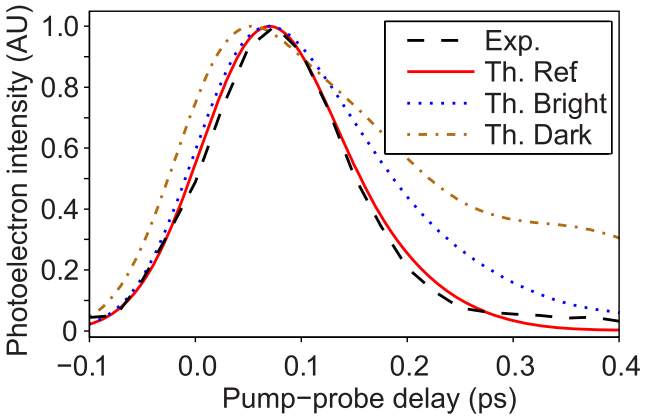

FIG. 9. TRPES intensity of BD at 2.5 eV electron kinetic energy with 216-nm pump and 267-nm probe wavelengths. The S_1 population is monitored exclusively by two-photon ionization in this energy range. Experimental data (dashed black curve) are compared to the theoretical results from three sets of simulations: SA-3-CAS(4/4)-MSPT2 reference electronic structure (solid red), SA-2-CAS(2/2)-MSPT2 bright-biased electronic structure (dotted blue), and SA-2-CAS(4/4)-MSPT2 dark-biased electronic structure (dot-dashed brown). All intensities have been normalized to a peak value of 1.

IV. CONCLUSIONS

In this paper, we simulated the excited state dynamics of BD and validated the simulations by direct comparison to TRPES spectra. Our simulations include both static and dynamic electron correlation effects with multistate perturbation theory (MSPT2), simultaneous with quantum nuclear effects corresponding to non-adiabatic transitions using *ab initio* multiple spawning (AIMS).

Our reference electronic structure method, SA-3-CAS(4/4)-MSPT2, provides a balanced treatment of bright and dark states and yields an excited-state mechanism which fully corroborates earlier simulations.[19] Namely, upon excitation to the initially planar 1^1B_u state, a large amplitude motion involving torsion around a terminal C–C bond leads, at larger twist angles, to an ultrafast transition between S_2 and S_1 with population split between (i) a channel involving a 1^1B_u-2^1A_g non-adiabatic transition and (ii) channels involving CT states at fully twisted terminal methylene geometries (Me^- and Me^+). In addition, simulated TRPES spectra calculated using our reference high-level electronic structure show excellent agreement with the experimental results presented and discussed in Paper I.[14] We demonstrated that the early time large amplitude terminal torsion motion on the ^1B_u state has a direct connection to the experimentally observable TRPES spectrum in the form of a sloped early time $(1 + 1')$ TRPES signal. As detailed in Paper I,[14] we suggest that this motion is the origin of the extreme breadth seen in the BD UV absorption spectrum. The S_1-S_0 transition also occurs on a <100-fs time scale and population decay is split between valence-character (transoid) and CT intersections (Me^- and Me^+), with the Me^- and transoid MECIs being roughly equally probable.

In order to better understand the role of the bright and dark states (i.e., S_1 and S_2) in the excited state dynamics of butadiene, we also considered two intentionally biased electronic structure methods. These involve energetically stabilizing either the bright state [SA-2-CAS(2/2)-MSPT2] or the dark state [SA-2-CAS(4/4)-MSPT2]. Simulations carried out with these biased methods can be thought of as representing the two previous competing paradigms of BD excited state dynamics. In particular, the bright-biased electronic structure is similar to Salem's 3×3 model CI Hamiltonian for BD and the predominance of the Me^- deactivation pathway at this level of theory is consistent with the mechanism put forward by Salem.[8] This bright-biased method is also similar to previous restricted open-shell Kohn-Sham-density functional theory (ROKS-DFT) treatments of BD excited state

dynamics,[16] since electronic structure methods restricted to single excitations such as restricted open-shell Kohn-Sham (ROKS)[64] or adiabatic linear-response time-dependent density functional theory (TDDFT)[65–67] are unable to describe the dark 2^1A_g state. On the other hand, the dark-biased electronic structure is similar to that used by Aoyagi[17] and Olivucci and co-workers,[10] who put forward a mechanism for BD non-radiative decay involving radicaloid hula-twist-like CI geometries (transoid).

Interestingly, we find neither the bright-biased nor the dark-biased simulations agree with experiment: both substantially overestimate the excited-state lifetime by roughly a factor of 2. This suggests that neither of the limiting bright/dark mechanisms can adequately describe BD's excited-state dynamics. Only an electronic structure method that places the bright and dark states in close energetic proximity gives good agreement with experiment. We suggest that the close proximity of bright and dark states in BD gives rise to a larger volume of energetically accessible S_1-S_0 seam space than would be the case for seams involving the bright state or dark state alone, explaining why the non-adiabatic transition in our reference electronic structure simulations is more efficient than either of the bright-biased or the dark-biased simulations. The existence of S_1-S_0 transitions occurring at geometries with simultaneously bright and dark character, i.e., Me^-/transoid and Me^+/transoid, further supports this idea.

Our proposed mechanism is also fully consistent with the rationalization of polyene photoproducts in terms of hula-twist (HT) mechanisms rather than one-bond flip (OBF) mechanisms.[3] Although the pure Me^- and Me^+ channels involve an OBF pathway, our simulations show that CT character can occur simultaneously with a HT pathway, i.e., via Me^-/transoid or Me^+/transoid transitions that occur midway on the S_1-S_0 seam.

We note that while our reference electronic structure simulations of BD show excellent agreement with experiment, there is certainly room for improvement. In particular, by treating only three states simultaneously, our calculations may be biased against the Me^+ state (which tends to be S_3 at the fully twisted terminal methylene C_s geometry). Although our calculations are capable of describing the Me^+ state following any geometric distortion which lowers it to S_2 or S_1, it would be preferable to treat it on equal footing with the other states. We did attempt simulations at the SA-4-CAS(4/4)-MSPT2 level of theory. However, those calculations were hampered for two reasons: first, S_3 is energetically much higher than S_2 at the FC geometry and, during dynamics, this state exhibits multiple crossings with higher lying states, giving rise to orbital discontinuities as described in Ref. 68. Second, the Me^- and Me^+ states, being both CT in character, have a similar splitting at the CASSCF and MSPT2 levels such that their mutual MSPT2 intersections are close in geometry to their CASSCF intersections, giving rise to well-known artifacts in the PES.[32,69] Extended multistate CASPT2 (XMSPT2) has been proposed to fix the latter problem,[32] and future work might explore the applicability of SA-4-CAS(4/4)-XMSPT2 to better describe the non-adiabatic dynamics of BD.

Taking together the experimental TRPEPICO results of Paper I[14] and the AIMS results of this paper, we believe that the controversies surrounding BD excited state dynamics are now largely resolved. We summarize the key points. (1) The TRPEPICO results show clear evidence for the elusive dark 2^1A_g state that is populated in a sequential manner during photodeactivation to the ground-state following non-adiabatic transitions from the bright 1^1B_u state. This finding suggests that the 2^1A_g state actually lies *below* the 1^1B_u state, at least for some regions of the potential energy surfaces accessed during the excited state dynamics. The AIMS simulations confirm this finding, albeit with the refinement that the bright state can also bypass the dark 2^1A_g state and instead undergo a non-adiabatic transition directly to the ground state, i.e., both bright and dark pathways (and hybrids of these) are followed simultaneously. (2) Large amplitude torsional (twisting) motion on the bright state is responsible for the extreme broadening seen in the UV absorption spectrum of BD. This motion precedes the non-adiabatic crossing to the dark state that occurs away from the FC region, at large twist angles. (3) The predictions of Levine and Martínez[19] that BD follows both bright and dark pathways in its non-radiative decay are confirmed by our higher-level MSPT2 AIMS simulations. Furthermore, only electronic structures that yield a small energy gap between the 1^1B_u and 2^1A_g states are able to accurately reproduce the experimental TRPES observables. In sum, we believe that BD can therefore truly be considered intermediate (or mixed) in behavior between localized ethylene-like and delocalized polyene-like excited-state dynamics.

SUPPLEMENTARY MATERIAL

See supplementary material for details of the coordinate system used to define torsion and pyramidalization angles, atomic coordinates for critical point geometries, and an example Molpro input deck for computing Dyson orbitals.

ACKNOWLEDGMENTS

The authors thank Christian Evenhuis and Hongli Tao for helpful discussions. This work was supported by the AMOS program within the Chemical Sciences, Geosciences and Biosciences Division of the Office of Basic Energy Sciences, Office of Science, U.S. Department of Energy. A.S. and M.S.S. thank the NSERC Discovery Grants program for financial support.

[1] R. S. H. Liu, "Photoisomerization by hula-twist: A fundamental supramolecular photochemical reaction," Acc. Chem. Res. **34**, 555 (2001).
[2] B. G. Levine and T. J. Martínez, "Isomerization through conical intersections," Annu. Rev. Phys. Chem. **58**, 613 (2007).
[3] W. Fuß, "Hula-twist cis-trans isomerization: The role of internal forces and the origin of regioselectivity," J. Photochem. Photobiol., A **237**, 53 (2012).
[4] T. Martinez, "Insights for light-driven molecular devices from *ab initio* multiple spawning excited-state dynamics of organic and biological chromophores," Acc. Chem. Res. **39**, 119 (2006).
[5] A. Warshel, "Bicycle-pedal model for the first step in the vision process," Nature **260**, 679 (1976).
[6] M. Ben-Nun, F. Molnar, H. Lu, J. C. Phillips, T. J. Martínez, and K. Schulten, "Quantum dynamics of the femtosecond photoisomerization of retinal in bacteriorhodopsin," Faraday Discuss. **110**, 447 (1998).

[7] P. Kukura, D. W. McCamant, S. Yoon, D. B. Wandschneider, and R. A. Mathies, "Structural observation of the primary isomerization in vision with femtosecond-stimulated Raman," Science **310**, 1006 (2005).

[8] P. Bruckmann and L. Salem, "Coexistence of two oppositely polarized zwitterionic forms on the lowest excited singlet surface of terminally twisted butadiene. Two-funnel photochemistry with dual stereochemistry," J. Am. Chem. Soc. **98**, 5037 (1976).

[9] V. Bonacic-Koutecky, M. Persico, D. Dohnert, and A. Sevin, "CI study of geometrical relaxation in the excited-states of butadiene. Energy surfaces and properties for simultaneous torsion and elongation of one double-bond," J. Am. Chem. Soc. **104**, 6900 (1982).

[10] M. Olivucci, I. N. Ragazos, F. Bernardi, and M. A. Robb, "A conical intersection mechanism for the photochemistry of butadiene. A MC-SCF study," J. Am. Chem. Soc. **115**, 3710 (1993).

[11] T. K. Allison, H. Tao, W. J. Glover, T. W. Wright, A. M. Stooke, C. Khurmi, J. van Tilborg, Y. Liu, R. W. Falcone, T. J. Martínez, and A. Belkacem, "Ultrafast internal conversion in ethylene. II. Mechanisms and pathways for quenching and hydrogen elimination," J. Chem. Phys. **136**, 124317 (2012).

[12] T. Mori, W. J. Glover, M. S. Schuurman, and T. J. Martínez, "Role of Rydberg states in the photochemical dynamics of ethylene," J. Phys. Chem. A **116**, 2808 (2011).

[13] H. Tao, T. K. Allison, T. W. Wright, A. M. Stooke, C. Khurmi, J. van Tilborg, Y. Liu, R. W. Falcone, A. Belkacem, and T. J. Martínez, "Ultrafast internal conversion in ethylene. I. The excited state lifetime," J. Chem. Phys. **134**, 244306 (2011).

[14] A. E. Boguslavskiy, O. Schalk, N. Gador, W. J. Glover, T. Mori, T. Schultz, M. S. Schuurman, T. J. Martinez, and A. Stolow, "Excited state nonadiabatic dynamics of the smallest polyene, *trans* 1,3-butadiene. I. Time-resolved photoelectron-photoion coincidence spectroscopy," J. Chem. Phys. **148**, 164302 (2018).

[15] P. Strodel and P. Tavan, "A revised MRCI-algorithm coupled to an effective valence-shell Hamiltonian. II. Application to the valence excitations of butadiene," J. Chem. Phys. **117**, 4677 (2002).

[16] C. Nonnenberg, S. Grimm, and I. Frank, "Restricted open-shell Kohn–Sham theory for π-π^* transitions. II. Simulation of photochemical reactions," J. Chem. Phys. **119**, 11585 (2003).

[17] M. Aoyagi and Y. Osamura, "A theoretical study of the potential energy surface of butadiene in the excited states," J. Am. Chem. Soc. **111**, 470 (1989).

[18] M. A. Watson and G. K.-L. Chan, "Excited states of butadiene to chemical accuracy: Reconciling theory and experiment," J. Chem. Theory Comput. **8**, 4013 (2012).

[19] B. G. Levine and T. J. Martínez, "*Ab initio* multiple spawning dynamics of excited butadiene: Role of charge transfer," J. Phys. Chem. A **113**, 12815 (2009).

[20] A. Komainda, B. Ostojić, and H. Köppel, "*Ab initio* quantum study of nonadiabatic S_1–S_2 photodynamics of *s-trans*-butadiene," J. Phys. Chem. A **117**, 8782 (2013).

[21] A. Komainda, D. Lefrancois, A. Dreuw, and H. Köppel, "Theoretical study of the initial non-radiative 1 $B_u \rightarrow 2$ A_g transition in the fluorescence quenching of s-*trans*-butadiene: Electronic structure methods and quantum dynamics," Chem. Phys. **482**, 27 (2017).

[22] H. Tao, B. G. Levine, and T. J. Martínez, "*Ab initio* multiple spawning dynamics using multi-state second-order perturbation theory," J. Phys. Chem. A **113**, 13656 (2009).

[23] T. S. Kuhlman, W. J. Glover, T. Mori, K. B. Moller, and T. J. Martínez, "Between ethylene and polyenes—The non-adiabatic dynamics of *cis*-dienes," Faraday Discuss. **157**, 193 (2012).

[24] L. Liu, J. Liu, and T. J. Martinez, "Dynamical correlation effects on photoisomerization: *Ab initio* multiple spawning dynamics with MS-CASPT2 for a model *trans*-protonated Schiff base," J. Phys. Chem. B **120**, 1940 (2016).

[25] T. J. Martínez, M. Ben-Nun, and R. D. Levine, "Molecular collision dynamics on several electronic states," J. Phys. Chem. A **101**, 6389 (1997).

[26] B. Levine, J. Coe, A. Virshup, and T. Martínez, "Implementation of *ab initio* multiple spawning in the Molpro quantum chemistry package," Chem. Phys. **347**, 3 (2008).

[27] J. Finley, P. Malmqvist, B. Roos, and L. Serrano-Andrés, "The multi-state CASPT2 method," Chem. Phys. Lett. **288**, 299 (1998).

[28] P. Celani and H. J. Werner, "Analytical energy gradients for internally contracted second-order multireference perturbation theory," J. Chem. Phys. **119**, 5044 (2003).

[29] T. Mori and S. Kato, "Dynamic electron correlation effect on conical intersections in photochemical ring-opening reaction of cyclohexadiene: MS-CASPT2 study," Chem. Phys. Lett. **476**, 97 (2009).

[30] H. Werner, P. Knowles, R. Lindh, F. Manby, and M. Schütz, MOLPRO, version 2006.2, a package of *ab initio* programs, 2006, see http://www.molpro.net.

[31] M. Schreiber, M. R. Silva-Junior, S. P. A. Sauer, and W. Thiel, "Benchmarks for electronically excited states: CASPT2, CC2, CCSD, and CC3," J. Chem. Phys. **128**, 134110 (2008).

[32] T. Shiozaki, W. Gyorffy, P. Celani, and H.-J. Werner, "Communication: Extended multi-state complete active space second-order perturbation theory: Energy and nuclear gradients," J. Chem. Phys. **135**, 081106 (2011).

[33] H.-J. Werner, P. J. Knowles, G. Knizia, F. R. Manby, M. Schütz, P. Celani, T. Korona, R. Lindh, A. Mitrushenkov, G. Rauhut, K. R. Shamasundar, T. B. Adler, R. D. Amos, A. Bernhardsson, A. Berning, D. L. Cooper, M. J. O. Deegan, A. J. Dobbyn, F. Eckert, E. Goll, C. Hampel, A. Hesselmann, G. Hetzer, T. Hrenar, G. Jansen, C. Köppl, Y. Liu, A. W. Lloyd, R. A. Mata, A. J. May, S. J. McNicholas, W. Meyer, M. E. Mura, A. Nicklass, D. P. O'Neill, P. Palmieri, D. Peng, K. Pflüger, R. Pitzer, M. Reiher, T. Shiozaki, H. Stoll, A. J. Stone, R. Tarroni, T. Thorsteinsson, and M. Wang, MOLPRO, version 2012.1, a package of *ab initio* programs, 2012, see http://www.molpro.net.

[34] H.-J. Werner, P. J. Knowles, G. Knizia, F. R. Manby, and M. Schütz, "Molpro: A general-purpose quantum chemistry program package," Wiley Interdiscip. Rev.: Comput. Mol. Sci. **2**, 242 (2012).

[35] B. G. Levine, J. D. Coe, and T. J. Martinez, "Optimizing conical intersections without derivative coupling vectors: Application to multistate multireference second-order perturbation theory (MS-CASPT2)," J. Phys. Chem. B **112**, 405 (2008).

[36] B. F. E. Curchod and T. J. Martínez, "*Ab initio* nonadiabatic quantum molecular dynamics," Chem. Rev. (published online).

[37] M. Ben-Nun and T. J. Martínez, "*Ab initio* quantum molecular dynamics," Adv. Chem. Phys. **121**, 439 (2002).

[38] A. L. Thompson, C. Punwong, and T. J. Martínez, "Optimization of width parameters for quantum dynamics with frozen Gaussian basis sets," Chem. Phys. **370**, 70 (2010).

[39] T. Shimanouchi, *Tables of Molecular Vibrational Frequencies. (Consolidated Volume 1)* (United States. National Bureau of Standards, 1972).

[40] C. Ciminelli, G. Granucci, and M. Persico, "The photoisomerization mechanism of azobenzene: A semiclassical simulation of nonadiabatic dynamics," Chem. - Eur. J. **10**, 2327 (2004).

[41] W. J. Glover, R. E. Larsen, and B. J. Schwartz, "The roles of electronic exchange and correlation in charge-transfer-to-solvent dynamics: Many-electron nonadiabatic mixed quantum/classical simulations of photoexcited sodium anions in the condensed phase," J. Chem. Phys. **129**, 164505 (2008).

[42] P. V. Parandekar and J. C. Tully, "Mixed quantum-classical equilibrium," J. Chem. Phys. **122**, 094102 (2005).

[43] J. D. Coe, M. T. Ong, B. G. Levine, and T. J. Martinez, "On the extent and connectivity of conical intersection seams and the effects of three-state intersections," J. Phys. Chem. A **112**, 12559 (2008).

[44] C. S. M. Allan, B. Lasorne, G. A. Worth, and M. A. Robb, "A straightforward method of analysis for direct quantum dynamics: Application to the photochemistry of a model cyanine," J. Phys. Chem. A **114**, 8713 (2010).

[45] O. Schalk, A. E. Boguslavskiy, and A. Stolow, "Two-photon excited state dynamics of dark valence, Rydberg, and superexcited states in 1,3-butadiene," J. Phys. Chem. Lett. **5**, 560 (2014).

[46] A. Makida, H. Igarashi, T. Fujiwara, T. Sekikawa, Y. Harabuchi, and T. Taketsugu, "Ultrafast relaxation dynamics in *trans*-1,3-butadiene studied by time-resolved photoelectron spectroscopy with high harmonic pulses," J. Phys. Chem. Lett. **5**, 1760 (2014).

[47] H. R. Hudock, B. G. Levine, A. L. Thompson, H. Satzger, D. Townsend, N. Gador, S. Ullrich, A. Stolow, and T. J. Martínez, "*Ab initio* molecular dynamics and time-resolved photoelectron spectroscopy of electronically excited uracil and thymine," J. Phys. Chem. A **111**, 8500 (2007).

[48] B. T. Pickup and O. Goscinski, "Direct calculation of ionization energies," Mol. Phys. **26**, 1013 (1973).

[49] B. T. Pickup, "On the theory of fast photoionization processes," Chem. Phys. **19**, 193 (1977).

[50] S. Patchkovskii, Z. Zhao, T. Brabec, and D. M. Villeneuve, "High harmonic generation and molecular orbital tomography in multielectron systems: Beyond the single active electron approximation," Phys. Rev. Lett. **97**, 123003 (2006).

[51] S. Gozem and A. I. Krylov, ezDyson, http://iopenshell.usc.edu/downloads/ezdyson, accessed 26 January.

[52] C. M. Oana and A. I. Krylov, "Dyson orbitals for ionization from the ground and electronically excited states within equation-of-motion coupled-cluster formalism: Theory, implementation, and examples," J. Chem. Phys. **127**, 234106 (2007).
[53] P. Å. Malmqvist, "Calculation of transition density matrices by nonunitary orbital transformations," Int. J. Quantum Chem. **30**, 479 (1986).
[54] The choice of exponent and displacement for the fictitious orbital represents the limiting values that Molpro accepts.
[55] J. E. Subotnik, S. Yeganeh, R. J. Cave, and M. A. Ratner, "Constructing diabatic states from adiabatic states: Extending generalized Mulliken-Hush to multiple charge centers with Boys localization," J. Chem. Phys. **129**, 244101 (2008).
[56] J. D. Coe, B. G. Levine, and T. J. Martínez, "*Ab initio* molecular dynamics of excited-state intramolecular proton transfer using multireference perturbation theory," J. Phys. Chem. A **111**, 11302 (2007).
[57] Due to the proximity of conical intersections, the S_2 geometry optimization used to generate Fig. 5(b) failed to converge at twisting angles of 60° and 90°. For these twist angles, we instead interpolated the geometries in internal Z-matrix coordinates using a cubic spline.
[58] We excluded the early time population dynamics from the fits in Fig. 7 due to there being both a waiting period before S_1-S_0 transitions and initial upward transitions from S_1 to S_2 states.
[59] U. Manthe and H. Köppel, "New method for calculating wave packet dynamics: Strongly coupled surfaces and the adiabatic basis," J. Chem. Phys. **93**, 345 (1990).
[60] U. Manthe and H. Köppel, "Dynamics on potential energy surfaces with a conical intersection: Adiabatic, intermediate, and diabatic behavior," J. Chem. Phys. **93**, 1658 (1990).
[61] M. Seel and W. Domcke, "Femtosecond time-resolved ionization spectroscopy of ultrafast internal-conversion dynamics in polyatomic molecules: Theory and computational studies," J. Chem. Phys. **95**, 7806 (1991).
[62] W. Domcke and G. Stock, "Theory of ultrafast nonadiabatic excited-state processes and their spectroscopic detection in real time," Adv. Chem. Phys. **100**, 1 (1997).
[63] C. Evenhuis and T. J. Martínez, "A scheme to interpolate potential energy surfaces and derivative coupling vectors without performing a global diabatization," J. Chem. Phys. **135**, 224110 (2011).
[64] I. Frank, J. Hutter, D. Marx, and M. Parrinello, "Molecular dynamics in low-spin excited states," J. Chem. Phys. **108**, 4060 (1998).
[65] D. J. Tozer and N. C. Handy, "On the determination of excitation energies using density functional theory," Phys. Chem. Chem. Phys. **2**, 2117 (2000).
[66] M. E. Casida and M. Huix-Rotllant, "Progress in time-dependent density functional theory," Annu. Rev. Phys. Chem. **63**, 287 (2012).
[67] A. Dreuw and M. Head-Gordon, "Single-reference *ab initio* methods for the calculation of excited states of large molecules," Chem. Rev. **105**, 4009 (2005).
[68] W. J. Glover, "Communication: Smoothing out excited-state dynamics: Analytical gradients for dynamically weighted complete active space self-consistent field," J. Chem. Phys. **141**, 171102 (2014).
[69] A. A. Granovsky, "Extended multi-configuration quasi-degenerate perturbation theory: The new approach to multi-state multi-reference perturbation theory," J. Chem. Phys. **134**, 214113 (2011).
[70] B. Efron and R. Tibshirani, "Bootstrap methods for standard errors, confidence intervals and other measures of statistical accuracy," Stat. Sci. **1**, 54 (1986).